

## Article

# Asymmetric Pt(II)-Porphyrin Incorporated in a PVC Ion-Selective Membrane for the Potentiometric Detection of Citrate

Dana Vlascici <sup>1,\*</sup>, Anca Lascu <sup>2,\*</sup> , Ion Fratilescu <sup>2</sup>, Diana Anghel <sup>2</sup>, Camelia Epuran <sup>2</sup>, Mihaela Birdeanu <sup>3,\*</sup> , Vlad Chiriac <sup>1</sup> and Eugenia Fagadar-Cosma <sup>2</sup> 

<sup>1</sup> Faculty of Chemistry, Biology, Geography, West University of Timisoara, 4 Vasile Parvan Ave, 300223 Timisoara, Romania

<sup>2</sup> Institute of Chemistry “Coriolan Dragulescu”, Mihai Viteazu Ave. 24, 300223 Timisoara, Romania

<sup>3</sup> National Institute for Research and Development in Electrochemistry and Condensed Matter, Plautius Andronescu Street 1, 300224 Timisoara, Romania

\* Correspondence: dana.vlascici@e-uvt.ro (D.V.); alascu@acad-icht.tm.edu.ro (A.L.); mihaelabirdeanu@gmail.com (M.B.)

**Abstract:** A new sensing material, Pt(II)-5-(4-carboxyphenyl)-10,15,20-tris(4-phenoxyphenyl)-porphyrin (Pt(II)-COOH-TPOPP), was synthesized and characterized. Polymeric membranes containing the porphyrin and three different plasticizers were used as an electroactive material for a new anion-selective sensor. The best composition of the membrane was the one plasticized with dioctylsebacate (DOS), the obtained sensor being citrate-selective in a linear range of  $5 \times 10^{-7}$ – $1 \times 10^{-1}$  M citrate. The slope was Nernstian (19.73 mV/decade) with good selectivity towards a number of interfering anions and a lifetime of five weeks.

**Keywords:** Pt-metalloporphyrin; A<sub>3</sub>B porphyrin; potentiometric sensor; PVC membrane; citrate ion detection



**Citation:** Vlascici, D.; Lascu, A.; Fratilescu, I.; Anghel, D.; Epuran, C.; Birdeanu, M.; Chiriac, V.; Fagadar-Cosma, E. Asymmetric Pt(II)-Porphyrin Incorporated in a PVC Ion-Selective Membrane for the Potentiometric Detection of Citrate. *Chemosensors* **2023**, *11*, 108. <https://doi.org/10.3390/chemosensors11020108>

Academic Editor: Tatsuo Yoshinobu

Received: 11 January 2023

Revised: 27 January 2023

Accepted: 31 January 2023

Published: 2 February 2023



**Copyright:** © 2023 by the authors. Licensee MDPI, Basel, Switzerland. This article is an open access article distributed under the terms and conditions of the Creative Commons Attribution (CC BY) license (<https://creativecommons.org/licenses/by/4.0/>).

## 1. Introduction

Citric acid and sodium citrate have been used since the early 1920s in the treatment of cow milk in order to increase the volatile acidity and to create butter [1]. Sodium citrate is used for the reduction of gastric acidity [2] and plays an important role in acid–base homeostasis and in preventing calcium nephrolithiasis [3]. The quantification of urinary citrate can be used as a marker for chronic kidney disease in patients suffering from autosomal dominant polycystic kidney disease [4]

Citrate is a known calcium chelating agent, it reduces ionic calcium in the blood, thus preventing coagulation. Because the bicarbonate dialysis fluid requires an acid to prevent precipitation of inorganic salts, replacing acetate with citrate improves hemodynamic stability, as it lowers the incidence of hypotension. Citrate can be used in lower doses and can improve the lean mass index of the patients [5]. Despite all the advantages of citrate intake, its accumulation in the blood, generating an increase in the  $Ca_{tot}/Ca^{2+}$  ratio as a side-effect of citrate anticoagulation treatment in patients with liver failure, has not been completely analyzed [6] and, therefore, the amount of net citrate load delivered to the patient during anticoagulation treatment should be minimized [7].

In industry, citrate ion is also a well-known reducing and capping agent in obtaining of noble-metal nanoparticles [8–11].

Over time, the detection of citrate has been performed by various instrumental methods, such as gas chromatography [12], spectrophotometry [13] and high-performance liquid chromatography [14]. Among these methods, potentiometric detection proved to be one of the most accurate.

Other frequently used methods for the detection of citrate ions are based on fluorometric measurements, especially for medical samples, as presented in Table 1.

**Table 1.** Sensitive materials used in the fluorometric detection of citrate.

Fluorophore	Concentration Domain (mol/L)/Medium	LOD (mol/L)	Ref.
Zn-triamino-guandine-thiophene (TAT)	0– $1.8 \times 10^{-6}$ In prostate cancer cells	$10.8 \times 10^{-9}$	[15]
Tetraphenyl-ethylene covalently linked to bipyridinium amide	$1-5 \times 10^{-6}$ Artificial urine	$1.0 \times 10^{-7}$	[16]
Triaminoguanidine carbon dots	0– $650 \times 10^{-9}$ Bioimaging in MCF-7 cells (breast epithelial cancer cells)	$4 \times 10^{-9}$	[17]

Methods for the detection of citrate are also based on the colorimetric response of the sensitive materials toward this anion. Thus, a colorimetric sensor based on silver nanoparticles capped with cetyl trimethyl ammonium bromide (CTAB) was reported [18]. In the case of naked-eye detection, the detected domain of citrate in urine was in the 1–130  $\mu\text{M}$  domain, with a limit of detection (LOD) of 25  $\mu\text{M}$ . By UV–Vis measurements, the detectable citrate concentration expanded up to 200  $\mu\text{M}$  and to a much lower limit of detection of 4.05 nM.

Another selective colorimetric chemosensor for citrate reported in the literature, this time from aqueous solutions, was based on a complex between a pyridylazo dye and  $\text{Ni}^{2+}$  in a 2:1 stoichiometric ratio [19]. The detected concentration domain was 1–100  $\mu\text{M}$ , with an LOD of 1.03  $\mu\text{M}$ .

A new and innovative method for the detection of citrate was reported, using an asymmetric double-opening ring metamaterial in terahertz (THz) spectroscopy [20]. This is a technique that can differentiate between several types of citrate salts (Zn, Ca, Mg, K, Li, Fe) in mM concentration ranges.

The electrochemical detection of fentanyl citrate was achieved by performing differential pulse voltammetry (DPV) using single-walled carbon nanotube network electrodes [21]. The fentanyl citrate concentration range that could be detected with accurate sensitivity and selectivity was 0.01–1  $\mu\text{M}$ , and the detection limit was calculated as 11 nM.

Porphyrins are some of the most remarkable ionophores known to date and have been extensively used in ion-selective polymeric membranes [22] for the potentiometric detection of heavy metals [23–25].

Platinum porphyrins are mainly used as catalysts in water oxidation [26,27], as oxygen nanosensors [28] for singlet oxygen generation [29–31], in the photodynamic therapy of cancer [32], as electron donors for organic solar cells [33] or as catalysts in water splitting [34].

An extensive study regarding anion-selective polymeric membrane electrodes using Pt(II)- and Pt(IV)-porphyrins as ionophores [35] determined the low oxophilicity of the central Pt-ion, and, thus, the capacity to avoid the dimerization of ionophore species in the membrane and, as a consequence, the super-Nernstian response of the electrodes.

Several aliphatic monatomic alcohols (ethanol, methanol and isobutyl alcohol) were detected by registering the potentiometric responses of Pt-porphyrin-based polymeric membranes [36]. The concentration range detected in all cases was from  $5.5 \times 10^{-5}$  M to 2.3 M. In order to validate the detection method, the authors tested the ethanol content of different beverages: grappa, whisky, various kinds of beer and dry wines.

Using Pt(II) 5,10,15,20-tetra(4-methoxy-phenyl)-porphyrin as an ionophore in plasticized membranes, the potentiometric detection of bromide ion was performed [37]. The bromide ion concentration range that produced a near-Nernstian potentiometric response of the sensor based on membranes plasticized with dioctylphthalate (DOP) was  $10^{-1}$  to  $10^{-5}$  M with a slope of  $(64.4 \pm 0.4)$  mV/decade and a detection limit of  $8 \times 10^{-6}$  M.

Using Pt(II)-5,10,15,20-tetra-(4-allyloxy-phenyl)porphyrin as a sensitive material in fluorescence, the lowest concentration of hydrogen peroxide was detected ( $1.05\text{--}3.9 \times 10^{-7}$  M) and the electrochemical method provided the widest detection domain ( $1 \times 10^{-6}$  M to  $5 \times 10^{-5}$  M) for the same analyte [38]. The incorporation of Pt(II)-5,10,15,20-tetra-(4-allyloxy-phenyl)-porphyrin into a silica matrix, based on tetraethylorthosilicate (TEOS), led to the achievement of a nanomaterial that is able to detect CO<sub>2</sub> gas in the concentration range 40–570 mM. The material performance to adsorb/recover CO<sub>2</sub> gas was one of the highest reported ( $25 \pm 0.05$  mmol CO<sub>2</sub>/g) [39].

Pt(II)-5-(3-hydroxy-phenyl)-10,15,20-tris-(3-methoxy-phenyl)-porphyrin complexed with gold nanoparticles was able to spectroscopically detect hydroquinone [34].

In this work we present the obtainment and characterization of a novel platinum- A<sub>3</sub>B mixed substituted metalloporphyrin, Pt(II)-5-(4-carboxyphenyl)-10,15,20-tris(4-phenoxyphenyl)-porphyrin, capable of performing as a suitable structured ionophore in PVC ion-selective membranes for the potentiometric detection of citrate anion.

## 2. Materials and Methods

### 2.1. Materials

Bis(benzonitrile)platinum(II) chloride PtCl<sub>2</sub>(PhCN)<sub>2</sub> was received from Alfa (Haverhill, Massachusetts, United States); sodium acetate CH<sub>3</sub>COONa × 3H<sub>2</sub>O was obtained from Sigma-Aldrich (St Louis, USA); chlorobenzene, dichloromethane and anhydrous sodium sulfate were purchased from Merck (Darmstadt, Germany). The methyl ester of 5-(4-carboxyphenyl)-10,15,20-tris(4-phenoxyphenyl)-porphyrin was synthesized using a mixture of methyl 4-formylbenzoate, 4-phenoxybenzaldehyde and pyrrole, in a molar ratio of 1/3/4, with propionic acid as the solvent in the presence of propionic anhydride. The final porphyrin derivative (COOH-TPOPP) was obtained by the hydrolyzation reaction of the methyl ester of porphyrin, conducted in strong basic conditions. Complete characterization of the (COOH-TPOPP) was reported in a previously published paper [40].

For membrane preparation, poly(vinyl)chloride (PVC) of high molecular weight was provided by Merck (Darmstadt, Germany). The three plastifiants, bis(2-ethylhexyl)sebacate (DOS), *o*-nitrophenyloctylether (NPOE) and dioctylphthalate (DOP), and the cationic additive tridodecylmethylammonium chloride (TDMACl) were also purchased from Merck (Darmstadt, Germany). All reagents were purum analyticum grade. In all measurements, double-distilled water was used.

### 2.2. Apparatus

UV-Vis spectra were acquired on a JASCO spectrophotometer V-650 model (Pfungstadt, Germany). For liquid samples, quartz cuvettes of 1 cm length were used.

Nuclear magnetic resonance spectra (NMR) were recorded on a Bruker Avance NEO 600 MHz apparatus (Rheinstetten, Germany). The samples were dissolved in deuterated chloroform (CDCl<sub>3</sub>). Tetramethylsilane was used as the reference and the chemical shifts  $\delta$  were noted in ppm.

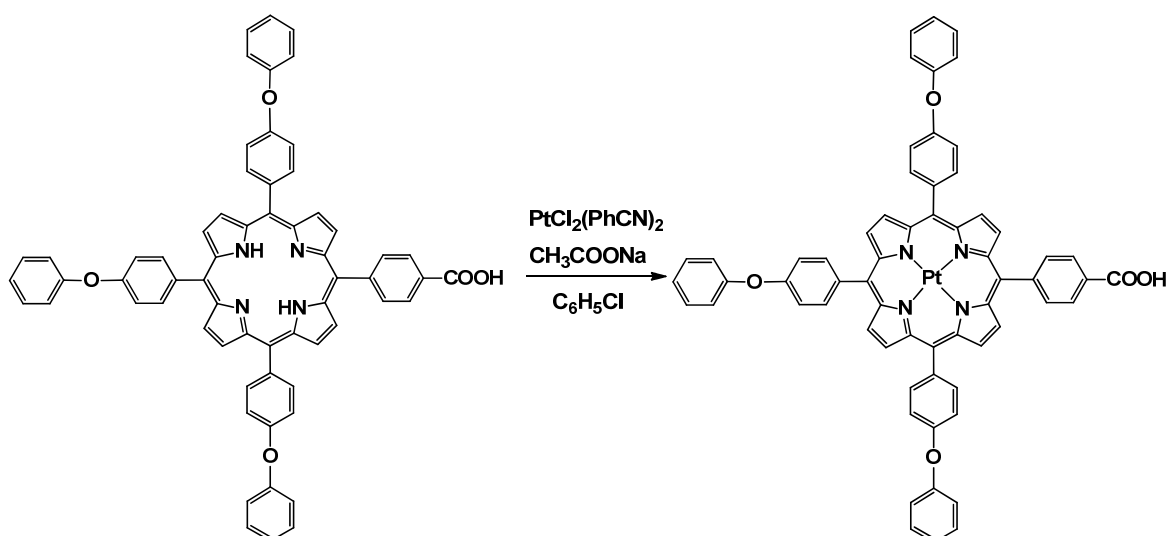
Infrared spectroscopy (FT-IR) samples were prepared as KBr pellets and recorded on a Jasco FT/IR-4200 model Type A device (Hachoji, Tokyo, Japan).

TGA/SDTA 851-LF 1100-Mettler equipment (Schwerzenbach, Switzerland) was employed for performing thermogravimetric analysis (TGA). The experiments were carried out under nitrogen atmosphere, using well ground powdered samples (about 5 mg each) deposited in Al crucibles, in a temperature domain varying from 25 °C up to 800 °C, with a heating rate of 10 °C min<sup>-1</sup>. After pyrolysis, the samples were maintained under isothermal conditions (800 °C) for 30 min in nitrogen and then in air atmosphere.

The presumed detection mechanism of the citrate ion was drawn using the optimized structure of Pt(II)-5-(4-carboxyphenyl)-10,15,20-tris(4-phenoxyphenyl)-porphyrin via the program PyMOLMolecular Graphics System, Version 1.7.4 Schrödinger (LLC New York, NY, USA, 2015).

### 2.3. Synthesis of Pt(II)-5-(4-Carboxyphenyl)-10,15,20-tris(4-phenoxyphenyl)-porphyrin (Pt(II)-COOH-TPOPP)

Pt(II)-COOH-TPOPP was synthesized by modifying previously reported methods [38,41–43], as follows (Scheme 1). The porphyrin base, 5-(4-carboxyphenyl)-10,15,20-tris(4-phenoxyphenyl)-porphyrin (COOH-TPOPP) (0.15 g,  $1.604 \times 10^{-4}$  mol) was dissolved in 35 mL of chlorobenzene and heated to reflux. A mixture composed of platinum complex  $\text{PtCl}_2(\text{PhCN})_2$  (0.1136 g,  $2.4063 \times 10^{-4}$  mol) and  $\text{CH}_3\text{COONa} \times 3\text{H}_2\text{O}$  (0.0873 g,  $6.4171 \times 10^{-4}$  mol) both dissolved in 15 mL of chlorobenzene was added dropwise. Sodium acetate was used to avoid decomposition of the platinum metalloporphyrin due to the formation of hydrochloric acid (HCl). The reflux was maintained for 80 min, taking samples for UV–Vis spectroscopy every 10 min. The reaction was stopped after UV–Vis spectra showed major changes in the number and location of the bands, namely, the reduction of the Q bands number and the hypsochromic shifting of the Soret band. The mixture was then filtered and the precipitate was repeatedly washed with large portions of warm water (100 mL). The filtrate was washed again in a separatory funnel with warm water ( $3 \times 200$  mL). The organic phase was dried over anhydrous  $\text{Na}_2\text{SO}_4$ , filtered and the solvent was evaporated under vacuum. The resulting product, (Pt(II)-COOH-TPOPP), was recrystallized from  $\text{CH}_2\text{Cl}_2$  and dried in an oven at  $105^\circ\text{C}$  for 24 h.



**Scheme 1.** Reaction scheme for obtaining Pt(II)-carboxy-phenyl-tris-(phenoxy-phenyl)porphyrin (Pt(II)-COOH-TPOPP).

The main characteristics of the obtained Pt(II)-5-(4-carboxyphenyl)-10,15,20-tris(4-phenoxyphenyl)-porphyrin: brownish-orange crystals; yield 92%; m.p. over  $300^\circ\text{C}$ ;  $^1\text{H-NMR}$  ( $\text{CDCl}_3$ , 600 MHz),  $\delta$  (ppm): 8.84–8.83 (d, 8H,  $\beta$ -pyrrole), 8.11–8.09 (d, 8H, 2,6-phenyl), 7.81–7.79 (d, 8H, 3,5-phenyl), 7.75–7.72 (t, 3H, 4\*-phenyl), 7.58–7.55 (t, 6H, 3\*,5\*-phenyl), 7.36–7.34 (d, 6H, 2\*,6\*-phenyl);  $^{13}\text{C-NMR}$  ( $\text{CDCl}_3$ , 600 MHz),  $\delta$  (ppm): 157.58 – 156.89 (C–O–C), 141.05 and 136.03 ( $\text{C}_{\alpha\text{-pyrrole}}$ ), 130.03 ( $\text{C}_{\beta\text{-pyrrole}}$ ), 119.62 ( $\text{C}_{\text{meso}}$  quaternary); **FT-IR** (KBr,  $\text{cm}^{-1}$ ): 793 ( $\nu_{\text{C-Hpyrrole}}$ ), 1105–1113 ( $\nu_{\text{C-O}}$ ), 1163 ( $\delta_{\text{N-H}}$ ), 1234 ( $\nu$  and  $\delta_{\text{Ar}}$  C–O–C), 1481 ( $\nu_{\text{C-O-C}}$  and  $\nu_{\text{C=N}}$ ), 1595–1592 ( $\nu_{\text{C=C}}$ ), 1677–1684 ( $\nu_{\text{COOas}}$ ), 2897–2916 ( $\nu_{\text{C-H}}$ ), 3424 ( $\nu_{\text{OH}}$ ); **UV–Vis**, DMSO ( $\lambda_{\text{max}}$ , nm (log  $\epsilon$ )): 406.1 (5.08), 511.4 (4.11), 541.5 (3.25), 596.7 (3.31).

### 2.4. Electrode Membrane Preparation and Measurements

The potentiometric investigations were conducted in a three-compartment cell, at environmental temperature on a pH/mV meter, model Hanna Instruments HI223. The cell notation is given below:

$\text{Hg} | \text{Hg}_2\text{Cl}_2 | \text{bridge electrolyte} | \text{sample} | \text{ion-selective membrane} | 0.01 \text{ M KCl} | \text{AgCl}, \text{Ag}$

This approach was based on the manufacturing of three membranes containing the metalloporphyrin ionophore, Pt(II)-COOH-TPOPP, PVC, and three plasticizers differen-

tiated by their polarity and their ability to modify the flexibility and durability of PVC at low temperature, such as *o*-nitrophenyloctylether (NPOE), dioctylphthalate (DOP) and dioctylsebacate (DOS). For the membrane composition, a lipophilic cationic additive was introduced in a ratio of 20 mol% relative to ionophore, namely, tridodecylmethylammonium chloride (TDMACl). The components were dissolved in 2 mL of tetrahydrofuran and vigorously stirred for 20 min. The three obtained solutions were poured onto a uniform plate glass and THF was allowed to completely evaporate in order to obtain flexible PVC membranes. Pieces of 8 mm diameter were cut out from each membrane and assembled on the Fluka electrode for further measurements. Before starting investigations, the sensors were conditioned for 48 h in 0.01 M citrate solution. Potentiometric selectivity coefficients were determined according to the separate solution method [44] by using the experimental EMF values obtained for 0.01 M solutions of the tested anions. The detection limit of the sensor was established at the point of intersection of the extrapolated linear range with the low concentration segment of the calibration plot.

### 3. Results and Discussion

#### 3.1. UV–Vis Monitoring of the Pt(II)-Carboxy-phenyl-tris-(phenoxy-phenyl)porphyrin Synthesis

The metalation process was monitored by UV–Vis spectroscopy, as presented in Figure 1. It can be observed that, during metalation, the Soret band located at 424 nm is initially decreasing in intensity and a shoulder appears at 406 nm, that is increasing in intensity as the process develops. Additionally, the QIV band is shifting hypsochromically, from 518 nm to 511 nm. It can be observed that the number of Q bands decreases to only 3.

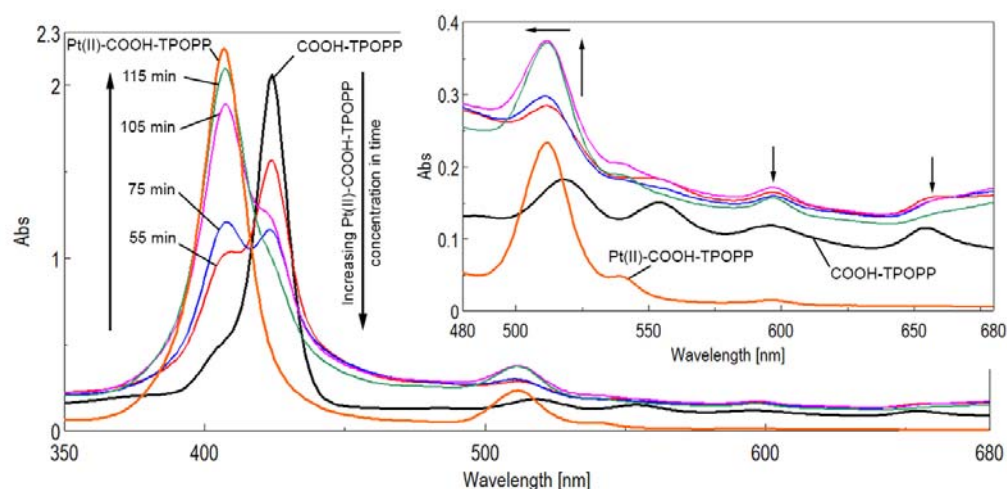


**Figure 1.** UV–Vis monitoring of the equilibria processes during the synthesis of Pt(II)-COOH-TPOPP. Details of the intermediate and final (orange) Q bands during the reaction are given. The arrows represent the hyperchromic, hypsochromic or blue shifting bands.

Analyzing the UV–Vis spectra of the carboxy-phenyl-tris-(phenoxy-phenyl)-porphyrin from chlorobenzene, it can be observed that it shows etio-type allure. The absorption spectrum presents an intense Soret band along with four Q bands in the visible region that are increasing in intensity in the order  $QI < QII < QIII < QIV$ . The Soret band at 426 nm is generated by the transition from  $a_{1u}(\pi)$  to  $e_g^*(\pi)$  and the four Q bands are the result of  $a_{2u}(\pi) - e_g^*(\pi)$  transitions. The Soret band of the metalated derivative is hypsochromically shifted by 18 nm, to 406 nm; the number of Q bands is diminished (Figure 2) to only 3, located at 511 nm with a pronounced shoulder at 541 nm and 597 nm, respectively.

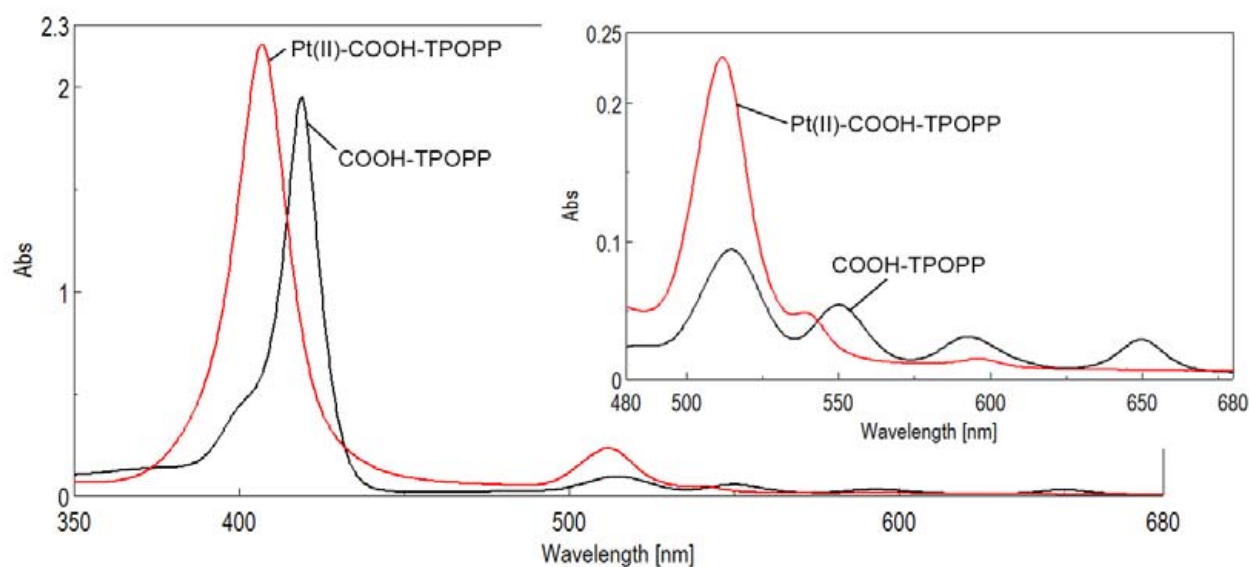


**Figure 2.** Overlapped UV–Vis spectra for carboxy-phenyl-*tris*-(phenoxy-phenyl)porphyrin (COOH-TPOPP) and Pt(II)-porphyrin (Pt(II)-COOH-TPOPP) from  $C_6H_5Cl$ . Details of the Q bands.

### 3.2. Nuclear Magnetic Resonance Characterization

The  $^1H$ -NMR spectrum is represented in Figure S1 (Supplementary Materials). The bonding of platinum in the inner core of the porphyrin is confirmed by the absence of the signal at  $-2.70$  ppm assigned to the two internal protons [40]. All the protons that prove the proposed structure are identified by their characteristic signals. Thus, the  $\beta$ -pyrrolic protons present a doublet in the  $8.84$ – $8.83$  ppm interval; the protons in the *para* position of the exterior phenyl ring give a triplet signal in the  $7.75$ – $7.72$  ppm region. The *meta* protons located in the exterior phenyl rings resonate as a triplet in the  $7.58$ – $7.55$  ppm domain. In the  $^{13}C$ -NMR spectrum presented in Figure S2 (Supplementary Materials), the main signals fairly correspond to attributed carbon atoms. The solvent (deuterated chloroform) gives a signal at  $77$  ppm. All aromatic carbons appear in the  $109$ – $157$  ppm region as assigned in Figure S2.

### 3.3. Comparative FT-IR-Analysis

In the FT-IR spectrum (Figure 3), the full metalation of the free-base porphyrin is confirmed in the spectrum by the absence of Pt-COOH-TPOPP of the peak representing the stretching vibration of the internal N-H bonds, located at  $3316\text{ cm}^{-1}$ . A comparison of the FT-IR spectra of the two compounds, the COOH-TPOPP porphyrin [40] and its platinum-derivative, gave some common features that can be noticed: the band located around  $3424\text{ cm}^{-1}$  represents the O-H stretching vibrations; the bands located at  $2897$ – $2916\text{ cm}^{-1}$  prove the symmetrical and asymmetrical stretching vibrations of the C-H bonds [45]. The peaks at  $1684$ – $1677\text{ cm}^{-1}$  and  $1105$ – $1113\text{ cm}^{-1}$  represent the -COO (asymmetric) and -C-O stretching vibrations, respectively [46]. The large band located around  $1595$ – $1592\text{ cm}^{-1}$  corresponds to the asymmetric stretching of the entire porphyrin macrocycle due to vibrations of the methyne bridges, of the pyrrole rings and of the symmetric C-C stretching in phenyl [47]. The band around  $1481\text{ cm}^{-1}$  is attributed to valence vibrations of C=N bonds [48]; the aromatic C-O-C bonds give an intense band at  $1234\text{ cm}^{-1}$  [49]. The  $1163\text{ cm}^{-1}$  vibration band is assigned to in-plane N-H bond deformation. The C-H pyrrole bond vibrates at  $793\text{ cm}^{-1}$  [50].

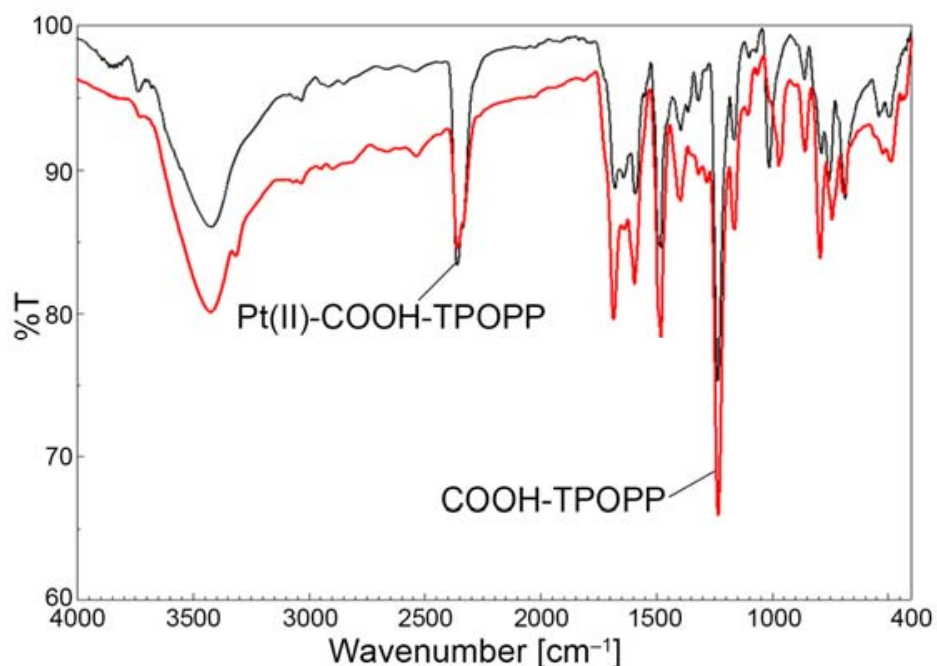


**Figure 3.** Overlapped FT-IR spectra of COOH-TPOPP and Pt(II)-COOH-TPOPP in KBr pellets.

#### 3.4. Thermogravimetric Analysis of COOH-TPOPP and Pt(II)-COOH-TPOPP

TGA provides information about the thermal stability of the two porphyrin derivatives. The TG/DTG/DTA curves of the studied compounds, porphyrin-base, COOH-TPOPP, and its metalloporphyrin, Pt(II)-COOH-TPOPP, are presented in Figures 4 and 5. Pt(II)-COOH-TPOPP exhibits a higher thermal stability than the porphyrin-base under an air atmosphere, a case that is similar to other reported investigations [51]. Both the thermal and the oxidative decomposition depend on the nature, number and position of the functional groups grafted on the porphyrin macrocycle. The decomposition of COOH-TPOPP has two distinctive stages, as can be seen in Figure 4: the second stage includes the decomposition of the porphyrin ring from around 300 to 800 °C. The porphyrin shows very good thermal stability up to 300 °C, the mass loss being less than 2%, but after that it begins to decompose [52].

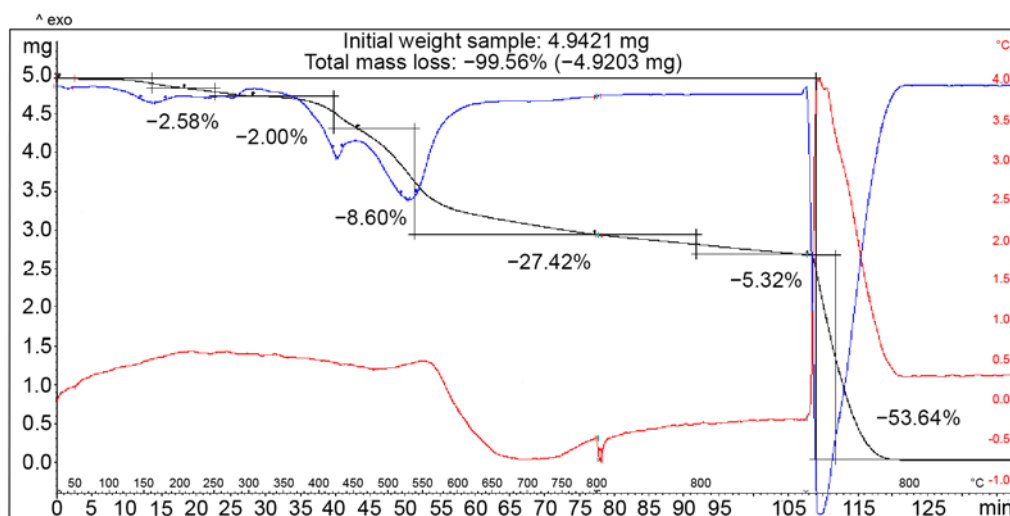


**Figure 4.** TGA diagrams of COOH-TPOPP decomposition.

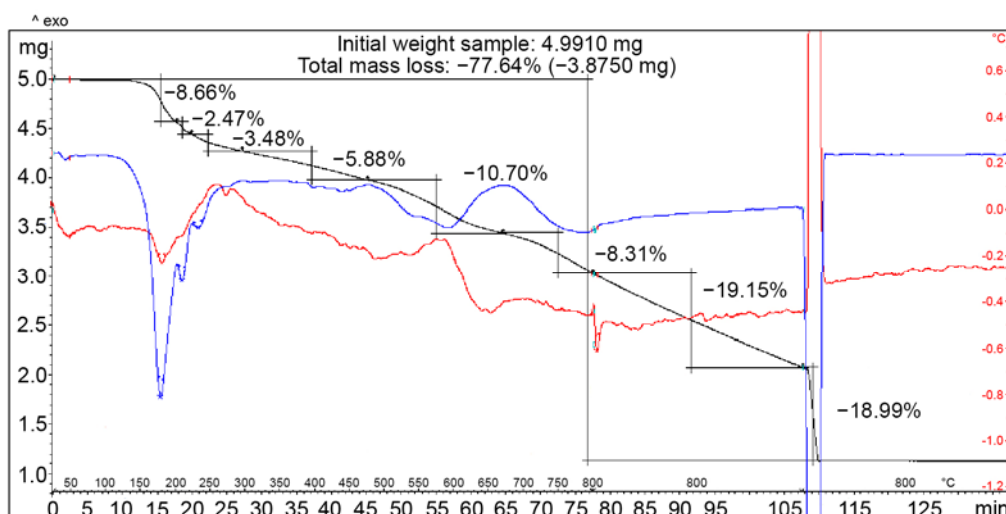


**Figure 5.** TGA diagrams of Pt(II)-COOH-TPOPP decomposition.

At 800 °C, under a nitrogen atmosphere, about 54% of the mass was lost. Under an air atmosphere at 800 °C, the decomposition reaction was almost completed, with a mass loss of 99.56%.

As opposed to the porphyrin base, in the case of metalloporphyrin Pt(II)-COOH-TPOPP, the TG curve (Figure 5) indicates a mass loss of 77.64%, both under nitrogen and air atmosphere. The thermal degradation occurs under a large exothermic peak in the DTA curve at 800 °C and can be associated with a combustion process of organic mass [53].

The thermogram of Pt-metalloporphyrin shows a 14.57% (0.73 mg) loss of mass in the range of 25 °C to 300 °C, which can be attributed to the presence of chlorobenzene solvent in the Pt(II)-COOH-TPOPP molecule. Differential thermal analysis (DTA) confirmed the presence of chlorobenzene solvent (e.g., endothermic peak with a maximum at 178.9 °C), as seen in the TG results.

Residual mass consisting in platinum(IV) oxide (PtO<sub>2</sub>), obtained during thermal decomposition after pyrolysis and heating in an air atmosphere at 800 °C, represents 22.4% (1.12 mg) of its initial mass.

The incorporation of chlorobenzene in the crystalline structure of Pt(II)-COOH-TPOPP could be evidenced both in the <sup>1</sup>H-NMR spectrum and in the thermogravimetric analysis. For the detection experiments, the Pt(II)-COOH-TPOPP compound was further dried and purified.

### 3.5. Potentiometric Detection

Using the newly obtained Pt(II)-COOH-TPOPP as an ionophore, three different plasticized PVC ion-selective sensors having the composition mentioned in Table 2 were formulated.

**Table 2.** The sensors' membrane composition (%w/w).

Membrane Composition.	Sensor 1	Sensor 2	Sensor 3
Ionophore	1	1	1
Plasticizer	DOS	66	
	DOP	66	
	NPOE		66
PVC	33	33	33

The used plasticizers, with three different dielectric constants, were o-nitrophenyloctylether (o-NPOE,  $\epsilon = 24$ ), dioctyl phthalate (DOP,  $\epsilon = 7$ ) and dioctyl sebacate (DOS,  $\epsilon = 4$ ). As we have

observed in our previous study [37], the cationic additive tridodecylmethylammonium chloride (TDMACl) was used as an additive (20 mol% relative to ionophore) due to the 2+ oxidation state of the central ion.

The performance of each sensor was investigated by measuring its potential in the concentration range  $10^{-6}$ – $10^{-1}$  M in 10 different anionic solutions:  $F^-$ ,  $Br^-$ ,  $I^-$ ,  $ClO_4^-$ ,  $SCN^-$ ,  $NO_2^-$ ,  $NO_3^-$ , Citrate $^{3-}$ ,  $Sal^-$ , Acetate $^-$ . Stock solutions of 0.1 M were prepared by dissolving sodium or potassium salts in a 4-morpholinoethanesulfonic acid (MES) buffer of pH 5.5 and also in Tris buffer of pH 8. All working solutions were prepared by gradual dilution of the stock solutions with the above-mentioned buffers.

Citric acid ( $H_3C_6H_5O_7$ ) is a tribasic acid with  $pK_a$  values of 3.128, 4.761 and 6.396. In order to obtain the exact species distribution of citric acid, we plotted the mole fraction versus pH (Figure 6).

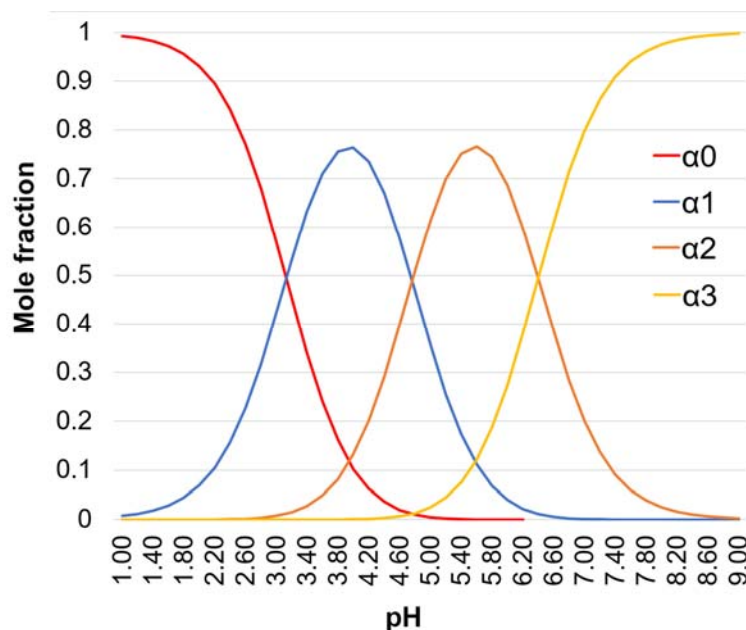


Figure 6. Citric acid distribution of species versus pH.

From Figure 6, we calculated the mole ratio of the species at each working pH, which is presented in Table 3.

Table 3. Mole ratio of citrate species at each working pH.

pH	$H_3Cit$	$H_2Cit^-$	$HCit^{2-}$	$Cit^{3-}$
5.50	-	1.46	7.93	1
8.00	-	-	1	39.8

The first measurements were made for all three sensors in solutions of pH 5.5. Analyzing the obtained measurements, it results that the best performances were obtained for Sensor 1 as a citrate-selective sensor, but only in the range of  $10^{-4}$ – $10^{-1}$  M citrate, with a slope of 35.4 mV/decade (instead of 29.6, the Nernstian value). As seen from Table 3, at pH 5.5 the most significant citrate species is  $HCit^{2-}$ , but the mole ratio with the other two species present in solution may be the reason for which the slope is bigger than Nernstian. For improving the DOS plasticized PVC sensor (Sensor 1), new measurements were made in Tris buffer solution of pH = 8. At this pH value, as resulting from Table 3, the main citrate species is  $C_6H_5O_7^{3-}$  in a mole ratio of 39.8:1, so a better fitted response towards the Nernstian slope can be expected for the potentiometric response.

Using the improved Sensor 1, the potentiometric responses for all the tested anions are illustrated in Figure 7.

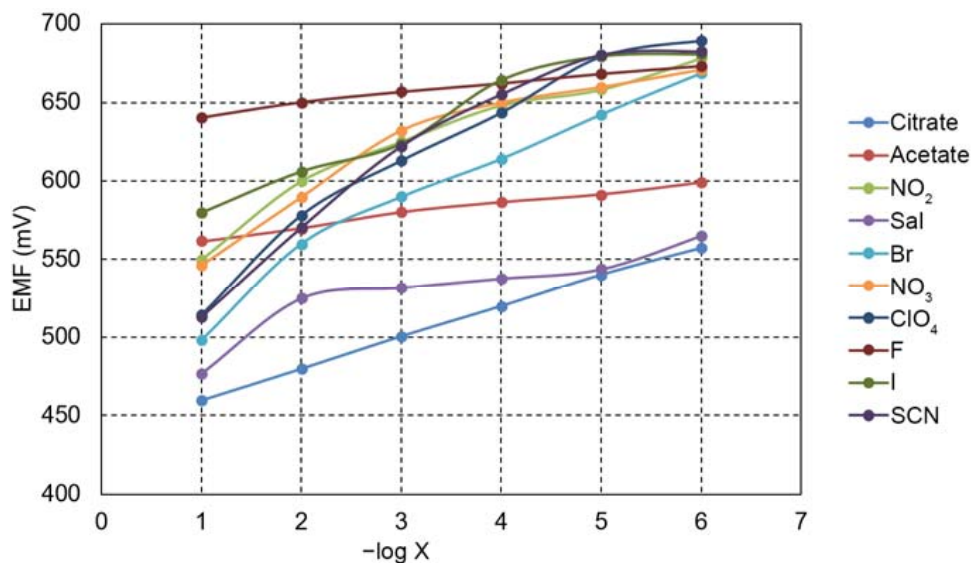


Figure 7. Potentiometric response of Sensor 1 to different anions.

A critical analysis of the results obtained in Figure 7 shows that the sensor is citrate-selective. To establish a more precise linear range of the sensor, a new dilution from  $10^{-6}$  to  $10^{-7}$  M was made and the new potentiometric results are presented in Figure 8. We can conclude that the sensor has a linear range from  $10^{-1}$  to  $5 \times 10^{-7}$  M, with an almost Nernstian slope of 19.73 mV/decade and a detection limit of  $3 \times 10^{-7}$  M.

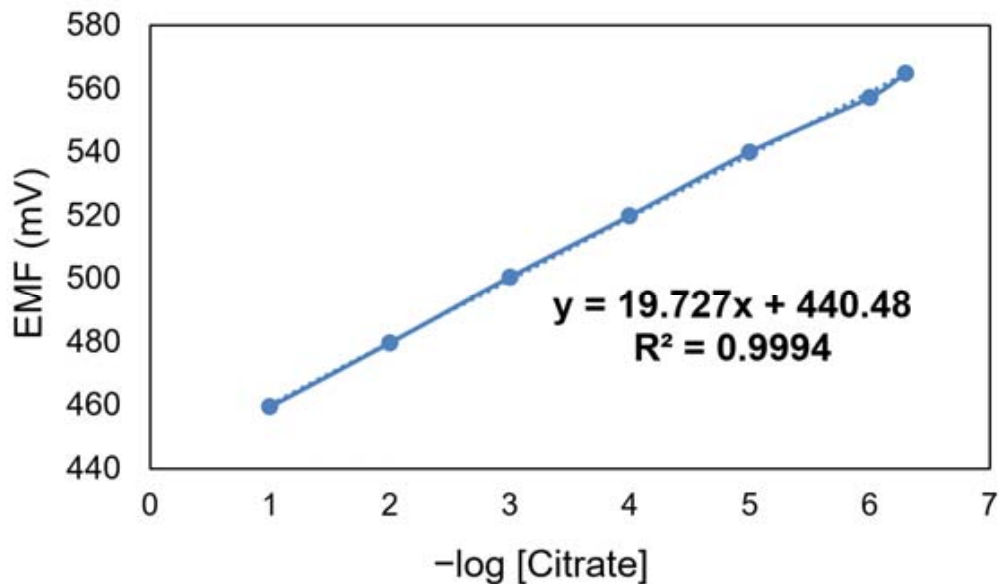
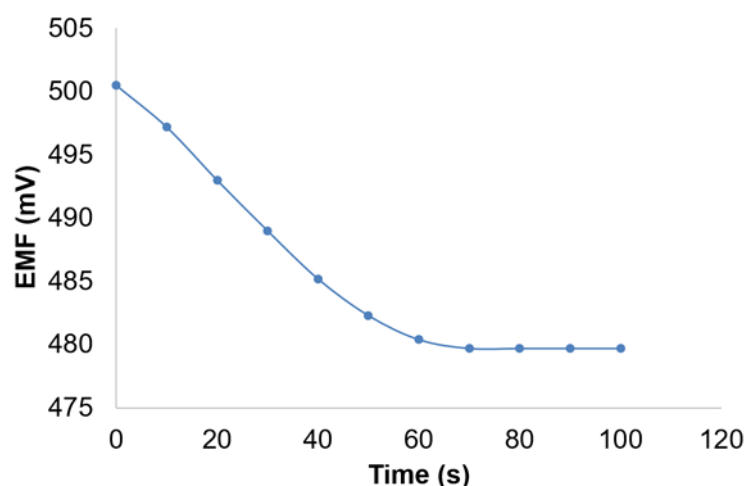


Figure 8. Potentiometric response of Sensor 1 toward citrate.

The response time of the sensor for citrate concentrations from  $10^{-3}$  to  $10^{-2}$  M is about 70 s, as presented in Figure 9.



**Figure 9.** Response time of Sensor 1.

The sensor was used for a period of 5 weeks without any significant change of the slope. After this period, a slight decrease in the slope was observed ( $17.5 \pm 0.5$  mV/decade).

The selectivity coefficients of the sensor were obtained by the separate solution method according to Equation (1) [44]:

$$\log K_{A,B}^{\text{pot}} = \frac{(E_B - E_A) \cdot z_A \cdot F}{R \cdot T \cdot \ln 10} + \left(1 - \frac{z_A}{z_B}\right) \cdot \lg a_A \quad (1)$$

where  $E_A$  and  $E_B$  are the potential values of the primary and interfering anions,  $a_A$  is the activity,  $z_A$  and  $z_B$  are the charge numbers of primary and interfering anions, and  $R$ ,  $T$  and  $F$  have their usual meaning.

Calculations were performed for equal concentrations of the primary and interfering anions, i.e.,  $10^{-2}$  M, and are presented in Table 4. The obtained values indicate a good selectivity toward citrate anion.

**Table 4.** Selectivity coefficients of Sensor 1 plasticized with DOS.

Anion	$\log K_{\text{Cit}, X}$
Ac <sup>-</sup>	$-(0.68 \pm 0.02)$
NO <sub>2</sub> <sup>-</sup>	$-(2.10 \pm 0.04)$
Sal <sup>-</sup>	$-(0.20 \pm 0.01)$
Br <sup>-</sup>	$-(0.40 \pm 0.02)$
NO <sub>3</sub> <sup>-</sup>	$-(1.59 \pm 0.04)$
F <sup>-</sup>	$-(4.64 \pm 0.05)$
I <sup>-</sup>	$-(2.41 \pm 0.05)$
SCN <sup>-</sup>	$-(0.60 \pm 0.02)$
ClO <sub>4</sub> <sup>-</sup>	$-(1.00 \pm 0.04)$

### 3.6. Presumed Mechanism of Citrate Recognition

The interactions between the porphyrin incorporated as a sensitive substance in the ion-selective membrane and the citrate anions occur mainly at the platinum atom located in the center of the porphyrin molecule. The following electrostatic interactions might take place as follows:

- Interactions between two opposite electrical charges (positively charged platinum coordinated in the porphyrin ring and negatively charged oxygen belonging to the carboxylate group contained in the citrate anion, depicted in yellow in Figure 10);
- $\pi$ -anion interactions between  $\pi$ -electrons of the extended aromatic heterocycle belonging to the porphyrin and the negatively charged oxygen from the carboxylate ion (represented in orange in Figure 10);

- $\pi$ - $\pi$  interaction between the non-participating electron pairs present both in the porphyrin macrocycle and in the carbonyl oxygen from citrate (green lines in Figure 10).

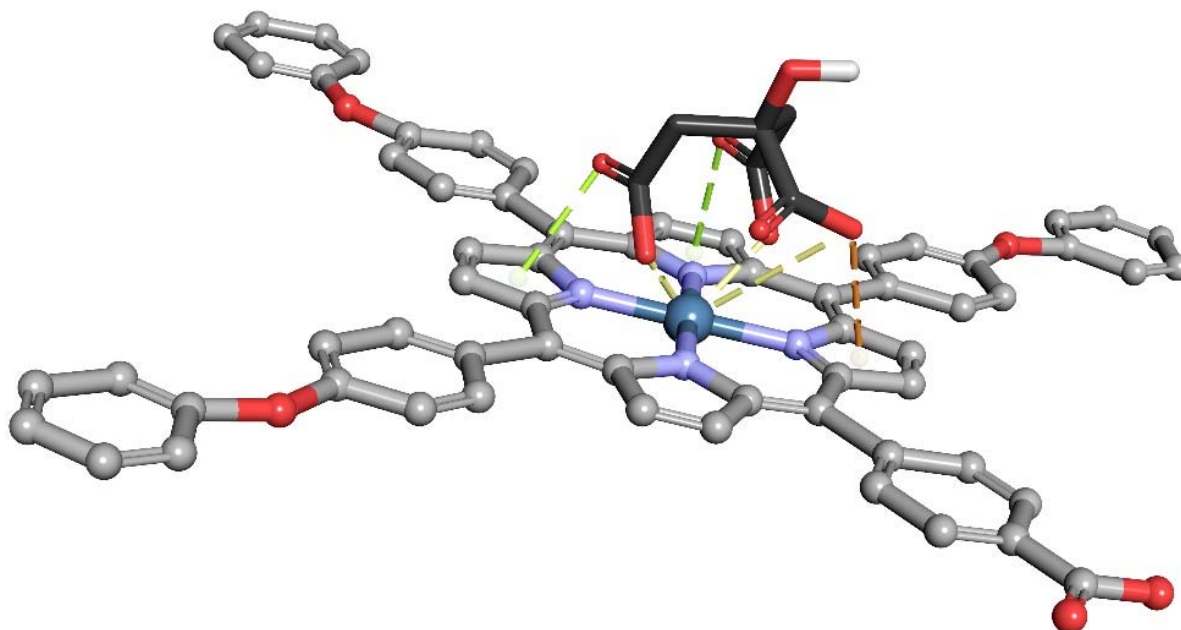


**Figure 10.** Illustrated interferences between the citrate ion and the Pt(II)-COOH-TPOPP used as an ionophore. The colors used for atom coding correspond to the standard CPK rules: carbon–black, oxygen–red, nitrogen–blue, platinum–dark blue, hydrogen–white.

Similar interactions were reported in literature [22,54,55] regarding tetraphenyl porphyrin-manganese(III) chloride as the ionophore and sulfadiazine the analyte [56] or Fe(III) tetrakis(pentafluorophenyl)porphyrin-chloride used in membrane formulation for the potentiometric detection of diclofenac [57].

### 3.7. Analytical Applications

The sensor was used with good results for the detection of citrate from synthetic samples and the obtained values are presented in Table 5.

**Table 5.** Analytical applications of sensors from synthetic samples.

Synthetic Sample	Amount (mg)	Found by Sensor (mg $\pm$ S <sup>a</sup> )
Citrate	200	198 $\pm$ 0.5
Citrate	600	597 $\pm$ 0.6

<sup>a</sup> Average of determinations on three samples of the same origin

Additionally, the sensor was used for the determination of citrate in food supplements, powders and tablets. The samples were prepared by dissolving them in Tris buffer of pH 8 and the citrate assay was carried out by direct potentiometry. The results are presented in Table 6 (average of three measurements) in comparison to the titration method. For the titration method, the samples were dissolved in distilled water and an aliquot was titrated with 0.05 M EDTA using ammonium buffer of pH 10 and Erio T as the indicator. The results are in good agreement.

**Table 6.** Determination of citrate in food supplements.

Sample	Amount (mg)	Found by Sensor (mg)	Found by Titration (mg)
Magnesium citrate (Gym Beam)	500	498 ± 0.9	492 ± 2.0
Calcium citrate (Now)	800	795 ± 2.0	790 ± 3.0
Magnesium citrate (Solgar) tablets	200	197 ± 0.5	195 ± 2.0

<sup>a</sup> Average of determinations on three samples of the same origin

#### 4. Conclusions

Pt(II)-5-(4-carboxyphenyl)-10,15,20-tris(4-phenoxyphenyl) porphyrin was synthesized, characterized and used as ionophore to obtain a new citrate-selective sensor. The sensor works in a linear range from  $5 \times 10^{-7}$  to  $1 \times 10^{-1}$  M citrate, has a detection limit of  $3 \times 10^{-7}$  M, a good selectivity toward a number of anions and a fast response time of 70 s. It was used for a period of five weeks for the quantitative determination of citrate from synthetic samples and food supplements.

Other sensitive materials [58–61] used over time for the potentiometric detection of citrate ion, gave similar [59] or lower performances regarding LOD than our sensor, as can be seen in Table 7.

**Table 7.** Sensitive materials used in the potentiometric detection of citrate.

Sensitive Material/Type of Electrode	Polymeric Membrane/Plasticizer	Membrane Composition (wt%)	Detection Domain (mol/L)/Medium	LOD (mol/L)	Ref.
Nano-clinoptilolite particles stabilized with hexadecyltrimethyl ammonium (SMZ)	Polyvinyl chloride (PVC) /dioctyl phthalate (DOP)	SMZ/PVC/DOP = 10:30:60	$5.0 \times 10^{-5}$ – $5.0 \times 10^{-2}$ Pharmaceutical tablets	$1.3 \times 10^{-5}$	[58]
Graphene functionalized with zinc monoamino-phthalocyanine (ZnMAPc-G)	PVC / dioctyl sebacate (DOS)	PVC/DOS/ZnMAPc-G = 31.1: 58.9:10	$8 \times 10^{-7}$ – $1 \times 10^{-2}$ Pharmaceuticals	$5 \times 10^{-7}$	[59]
Bis(triphenyl-phosphoran-yliden) ammonium chloride (BTPIIA)	PVC / bis (2-ethylhexyl) sebacate (bEHS) / p-tert-octylphenol -(TOP)	BTPIIA/bEHS/ TOP/PVC = 1.3:60.6:6.5: 31.6	$1.0 \times 10^{-4}$ to $1.0 \times 10^{-2}$ Soft drinks and pharmaceuticals	$5 \times 10^{-5}$	[60]
Mono- and di-nuclear copper(II) complex with salicylaldehyde-semicarbazone ligand (CuLBr)	PVC / DOP, Trioctylmethyl ammonium chloride (MTOAC)	PVC/DOP/ CuLBr/MTOAC = 30.3: 62: 4: 3.7	$1.0 \times 10^{-7}$ – $1.0 \times 10^{-1}$ In juices	$6.3 \times 10^{-8}$	[61]
Pt(II)-5-(4-carboxyphenyl)-10,15,20-tris(4-phenoxyphenyl)-porphyrin (Pt(II)-COOH-TPOPP)	PVC / dioctyl sebacate (DOS)	Pt(II)-COOH-TPOPP/PVC/DOS = 1:33:66	$5.0 \times 10^{-7}$ – $1.0 \times 10^{-1}$ Synthetic samples and food supplements	$3 \times 10^{-7}$	This work

**Supplementary Materials:** The following supporting information can be downloaded at: <https://www.mdpi.com/article/10.3390/chemosensors11020108/s1>, Figure S1: The  $^1\text{H-NMR}$  spectrum of Pt(II)-COOH-TPOPP in  $\text{CDCl}_3$ ; Figure S2: The assignment of the main signals in the  $^{13}\text{C-NMR}$  spectrum of Pt(II)-COOH-TPOPP ( $\text{CDCl}_3$ ).

**Author Contributions:** Conceptualization, D.V. and E.F.-C.; methodology, D.V., A.L., M.B. and E.F.-C.; software, I.F., M.B. and V.C.; validation, D.V., V.C. and E.F.-C.; formal analysis, A.L., C.E., I.F., D.A. and M.B.; investigation, A.L., D.A., C.E., I.F. and M.B.; resources, E.F.-C.; data curation, A.L., I.F. and V.C.; writing—original draft preparation, D.V., A.L., I.F., V.C. and E.F.-C.; writing—review and editing, D.V. and E.F.-C.; visualization, A.L., I.F., C.E. and E.F.-C.; supervision, D.V. and E.F.-C.; project administration, E.F.-C.; funding acquisition, E.F.-C. All authors have read and agreed to the published version of the manuscript.

**Funding:** This research was funded by the Romanian Academy, through program 3/2023 from the Institute of Chemistry “Coriolan Dragulescu”, and developed some further applications previously funded by UEFISCDI, grant number 76 PCCDI/2018-ECOTECH-GMP.

**Institutional Review Board Statement:** Not applicable.

**Informed Consent Statement:** Not applicable.

**Data Availability Statement:** The data presented in this study are available on request from the first or the corresponding author.

**Acknowledgments:** The authors would like to acknowledge the Institute of Macromolecular Chemistry “Petru Poni” for providing the NMR spectra. The authors gratefully acknowledge Liliana Halip from the Institute of Chemistry “Coriolan Dragulescu” (Timisoara, Romania) for the optimized structures by using the program PyMOLMolecular Graphics System.

**Conflicts of Interest:** All authors declare that the research was conducted in the absence of any commercial or financial relationships that could be construed as a potential conflict of interest.

## References

1. Templeton, H.L.; Sommer, H.H. The Use of Citric Acid and Sodium Citrate in Starter Cultures. *J. Dairy Sci.* **1929**, *12*, 21–36. [[CrossRef](#)]
2. Viegas, O.J.; Ravindran, R.S.; Shumacker, C.A. Gastric fluid pH in patients receiving sodium citrate. *Anesth. Analg.* **1981**, *60*, 521–523. Available online: <http://www.anesthesia-analgia.org/cgi/content/abstract/60/7/521> (accessed on 30 January 2023). [[CrossRef](#)] [[PubMed](#)]
3. Weiner, I.D.; Verlander, J.W.; Wingo, C.S. Renal Acidification Mechanisms. In *Core Concepts in the Disorders of Fluid, Electrolytes and Acid-Base Balance*; Mount, D., Sayegh, M., Singh, A., Eds.; Springer: Boston, MA, USA, 2013; pp. 203–233. [[CrossRef](#)]
4. Borrego Utiel, F.J.; Herrera Contreras, I.; Merino García, E.M.; Camacho Reina, M.V.; Morina Dominguez, C.; Ocana Perez, E. Urinary citrate as a marker of renal function in patients with autosomal dominant polycystic kidney disease. *Int. Urol. Nephrol.* **2022**, *54*, 873–881. [[CrossRef](#)]
5. de Sequera, P.; Pérez-García, R.; Molina, M.; Álvarez-Fernández, G.; Muñoz-González, R.I.; Mérida, E.; Camba, M.J.; Blázquez, L.A.; Alcaide, M.P.; Echarri, R. Advantages of the use of citrate over acetate as a stabilizer in hemodialysis fluid: A randomized ABC-treat study. *Nefrologia* **2022**, *42*, 327–337. [[CrossRef](#)]
6. Schneider, A.G.; Journois, D.; Rimmelé, T. Complications of regional citrate anticoagulation: Accumulation or overload? *Crit. Care.* **2017**, *21*, 281. [[CrossRef](#)]
7. Thanapongsatorn, P.; Chaijamorn, W.; Sirivongrangson, P.; Tachaboon, S.; Peerapornratana, S.; Lumlertgul, N.; Lucksiri, A.; Srisawat, N. Citrate pharmacokinetics in critically ill liver failure patients receiving CRRT. *Sci. Rep.* **2022**, *12*, 1815. [[CrossRef](#)] [[PubMed](#)]
8. Mohaghegh, S.; Osouli-Bostanabad, K.; Nazemiyeh, H.; Javadzadeh, Y.; Parvizpur, A.; Barzegar-Jalali, M.; Adibkia, K. A comparative study of eco-friendly silver nanoparticles synthesis using *Prunus domestica* plum extract and sodium citrate reducing agents. *Adv. Powder Technol.* **2020**, *31*, 169–180. [[CrossRef](#)]
9. Grys, D.B.; de Nijs, B.; Salmon, A.R.; Huang, J.; Wang, W.; Chen, W.H.; Scherman, O.A.; Baumberg, J.J. Citrate Coordination and Bridging of Gold Nanoparticles: The Role of Gold Adatoms in AuNP Ageing. *ACS Nano.* **2020**, *14*, 8689–8696. [[CrossRef](#)] [[PubMed](#)]
10. Ally, N.; Hendricks, N.; Gumbi, B. A Colorimetric Detection of Noradrenaline in Wastewater Using Citrate-Capped Colloidal Gold Nanoparticles Probe. *Colloids Interfaces* **2022**, *6*, 61. [[CrossRef](#)]
11. Ali, M.; Khalid, M.A.U.; Shah, I.; Kim, S.W.; Kim, Y.S.; Lim, J.H.; Choi, K.H. Paper-based selective and quantitative detection of uric acid using citrate-capped Pt nanoparticles (PtNPs) as a colorimetric sensing probe through a simple and remote-based device. *New J. Chem.* **2019**, *43*, 7636–7645. [[CrossRef](#)]
12. DeBorba, B.M.; Rohrer, J.S.; Bhattacharyya, L. Development and validation of an assay for citric acid/citrate and phosphate in pharmaceutical dosage forms using ion chromatography with suppressed conductivity detection. *J. Pharm. Biomed. Anal.* **2004**, *36*, 517–524. [[CrossRef](#)]

13. Luque-Peréz, E.; Ríos, A.; Valcárcel, M. Flow-injection spectrophotometric determination of citric acid in beverages based on a photochemical reaction. *Anal. Chim. Acta* **1998**, *366*, 231–240. [[CrossRef](#)]
14. Morales, M.L.; Ferreira, R.; González, A.G.; Troncoso, A.M. Simultaneous determination of organic acids and sweeteners in soft drinks by ion-exclusion HPLC. *J. Sep. Sci.* **2001**, *24*, 879–884. [[CrossRef](#)]
15. Muthusamy, S.; Zhu, D.; Rajalakshmi, K.; Zhu, W.; Wang, S.; Lee, K.-B.; Zhao, L. Successive Detection of Zinc Ion and Citrate Using a Schiff Base Chemosensor for Enhanced Prostate Cancer Diagnosis in Biosystems. *ACS Appl. Bio. Mater.* **2021**, *4*, 1932–1941. [[CrossRef](#)]
16. Liu, C.; Hang, Y.; Jiang, T.; Yang, J.; Zhang, X.; Hua, J. A light-up fluorescent probe for citrate detection based on bispyridinium amides with aggregation-induced emission feature. *Talanta* **2018**, *178*, 847–853. [[CrossRef](#)] [[PubMed](#)]
17. Rajalakshmi, K.; Deng, T.; Muthusamy, S.; Xie, M.; Xie, J.; Lee, K.-B.; Xu, Y. Prostate cancer biomarker citrate detection using triaminoguanidinium carbon dots, its applications in live cells and human urine samples. *Spectrochim. Acta A Mol. Biomol. Spectrosc.* **2022**, *268*, 120622. [[CrossRef](#)]
18. Shaban, S.M.; Lee, J.Y.; Kim, D.-H. Dual-Surfactant-Capped Ag Nanoparticles as a Highly Selective and Sensitive Colorimetric Sensor for Citrate Detection. *ACS Omega* **2020**, *5*, 10696–10703. [[CrossRef](#)]
19. Fukushima, Y.; Aikawa, S. Colorimetric chemosensor based on a Ni<sup>2+</sup> complex of a pyridylazo dye for detection of citrate in aqueous solution. *Tetrahedron Lett.* **2020**, *61*, 151681. [[CrossRef](#)]
20. Deng, X.; Shen, Y.; Liu, B.; Song, Z.; He, X.; Zhang, Q.; Ling, D.; Liu, D.; Wei, D. Terahertz Metamaterial Sensor for Sensitive Detection of Citrate Salt Solutions. *Biosensors* **2022**, *12*, 408. [[CrossRef](#)] [[PubMed](#)]
21. Wester, N.; Mynttinen, E.; Etula, J.; Lilius, T.; Kalso, E.; Mikkladal, B.F.; Zhang, Q.; Jiang, H.; Sainio, S.; Nordlund, D.; et al. Single-Walled Carbon Nanotube Network Electrodes for the Detection of Fentanyl Citrate. *ACS Appl. Nano Mater.* **2020**, *3*, 1203–1212. [[CrossRef](#)]
22. Ozbek, O.; Isildak, O.; Berkel, C. The use of porphyrins in potentiometric sensors as ionophores. *J. Incl. Phenom. Macrocycl. Chem.* **2020**, *98*, 1–9. [[CrossRef](#)]
23. Vlascici, D.; Fagadar-Cosma, E.; Pica, E.M.; Cosma, V.; Bizerea, O.; Mihailescu, G.; Olenic, L. Free Base Porphyrins as Ionophores for Heavy Metal Sensors. *Sensors* **2008**, *8*, 4995–5004. [[CrossRef](#)]
24. Vlascici, D.; Popa, I.; Chiriac, V.A.; Fagadar-Cosma, G.; Popovici, H.; Fagadar-Cosma, E. Potentiometric detection and removal of copper using porphyrins. *Chem. Cent. J.* **2013**, *7*, 111. [[CrossRef](#)] [[PubMed](#)]
25. Taranu, B.O.; Vlascici, D.; Sebarchevici, I.; Fagadar-Cosma, E. The aggregation behavior of an A<sub>3</sub>B free base porphyrin and its application as chromium(III)-selective membrane sensor. *Stud. Univ. Babeş-Bolyai Chem. LXI* **2016**, *1*, 199–212.
26. Bodedla, G.B.; Dong, Y.; Tang, G.; Zhao, J.; Zhang, F.; Zhu, X.; Wong, W.-Y. Long-lived excited states of platinum(II)-porphyrins for highly efficient photocatalytic hydrogen evolution. *J. Mater. Chem. A* **2022**, *10*, 13402–13409. [[CrossRef](#)]
27. Orfanos, E.; Ladomenou, K.; Angaridis, P.A.; Papadopoulos, T.; Charalambidis, G.; Vasilopoulou, M.; Coutsolelos, A.G. A stable platinum porphyrin based photocatalyst for hydrogen production under visible light in water. *Sustain. Energy Fuels* **2022**, *6*, 5072–5076. [[CrossRef](#)]
28. Wang, X.; Peng, H.; Cheng, K.; Liu, X.; Liu, Y.; Yang, W. Two-photon oxygen nanosensors based on a conjugated fluorescent polymer doped with platinum porphyrins. *Methods Appl. Fluoresc.* **2018**, *6*, 035008. [[CrossRef](#)] [[PubMed](#)]
29. Garai, A.; Villa, M.; Marchini, M.; Patra, S.K.; Pain, T.; Mondal, S.; Ceroni, P.; Kar, S. Synthesis, Structure, Photophysics, and Singlet Oxygen Sensitization by a Platinum(II) Complex of Meso-Tetra-Acenaophthyl Porphyrin. *Eur. J. Inorg. Chem.* **2021**, *39*, 4089–4095. [[CrossRef](#)]
30. Subedi, D.R.; Reid, R.; D'Souza, P.F.; Nesterov, V.N.; D'Souza, F. Singlet Oxygen Generation in Peripherally Modified Platinum and Palladium Porphyrins: Effect of Triplet Excited State Lifetimes and meso-Substituents on <sup>1</sup>O<sub>2</sub> Quantum Yields. *ChemPlusChem* **2022**, *87*, e202200010. [[CrossRef](#)]
31. Yao, B.; He, Y.; Wang, S.; Sun, H.; Liu, X. Recent Advances in Porphyrin-Based Systems for Electrochemical Oxygen Evolution Reaction. *Int. J. Mol. Sci.* **2022**, *23*, 6036. [[CrossRef](#)]
32. Yang, M.; Deng, J.; Guo, D.; Zhang, J.; Yang, L.; Wu, F. A folate-conjugated platinum porphyrin complex as a new cancer-targeting photosensitizer for photodynamic therapy. *Org. Biomol. Chem.* **2019**, *17*, 5367–5374. [[CrossRef](#)]
33. Gao, Y.; Piradi, V.; Zhu, X.; So, S.K. Palladium(II) and Platinum(II) Porphyrin Donors for Organic Photovoltaics. *ACS Appl. Energy Mater.* **2022**, *5*, 4916–4925. [[CrossRef](#)]
34. Fratilesco, I.; Lascu, A.; Taranu, B.O.; Epuran, C.; Birdeanu, M.; Macsim, A.-M.; Tanasa, E.; Vasile, E.; Fagadar-Cosma, E. One A<sub>3</sub>B Porphyrin Structure—Three Successful Applications. *Nanomaterials* **2022**, *12*, 1930. [[CrossRef](#)]
35. Lvova, L.; Verrelli, G.; Stefanelli, M.; Nardis, S.; Di Natale, C.; D'Amico, A.; Makarychev-Mikhailov, S.; Paolesse, R. Platinum porphyrins as ionophores in polymeric membrane electrodes. *Analyst* **2011**, *136*, 4966–4976. [[CrossRef](#)] [[PubMed](#)]
36. Lvova, L.; Paolesse, R.; Di Natale, C.; D'Amico, A. Detection of alcohols in beverages: An application of porphyrin-based Electronic tongue. *Sens. Actuators B Chem.* **2006**, *118*, 439–447. [[CrossRef](#)]
37. Vlascici, D.; Plesu, N.; Fagadar-Cosma, G.; Lascu, A.; Petric, M.; Crisan, M.; Belean, A.; Fagadar-Cosma, E. Potentiometric Sensors for Iodide and Bromide Based on Pt(II)-Porphyrin. *Sensors* **2018**, *18*, 2297. [[CrossRef](#)] [[PubMed](#)]
38. Fagadar-Cosma, E.; Plesu, N.; Lascu, A.; Anghel, D.; Cazacu, M.; Ianasi, C.; Fagadar-Cosma, G.; Fratilesco, I.; Epuran, C. Novel Platinum-Porphyrin as Sensing Compound for Efficient Fluorescent and Electrochemical Detection of H<sub>2</sub>O<sub>2</sub>. *Chemosensors* **2020**, *8*, 29. [[CrossRef](#)]

39. Anghel, D.; Lascu, A.; Epuran, C.; Fratilescu, I.; Ianasi, C.; Birdeanu, M.; Fagadar-Cosma, E. Hybrid Materials Based on Silica Matrices Impregnated with Pt-Porphyrin or PtNPs Destined for CO<sub>2</sub> Gas Detection or for Wastewaters Color Removal. *Int. J. Mol. Sci.* **2020**, *21*, 4262. [[CrossRef](#)] [[PubMed](#)]
40. Vlascici, D.; Fagadar-Cosma, E.; Popa, I.; Chiriac, V.; Gil-Augusti, M. A Novel Sensor for Monitoring of Iron(III) Ions Based on Porphyrins. *Sensors* **2012**, *12*, 8193–8203. [[CrossRef](#)]
41. Yamashita, K.; Katsumata, N.; Tomita, S.; Fuwa, M.; Fujimaki, K.; Yoda, T.; Hirano, D.; Sugiura, K. Facile and practical synthesis of platinum(II) porphyrins under mild conditions. *Chem. Lett.* **2015**, *44*, 492–494. [[CrossRef](#)]
42. Fagadar-Cosma, E.; Lascu, A.; Shova, S.; Zaltariov, M.-F.; Birdeanu, M.; Croitor, L.; Balan, A.; Anghel, D.; Stamatina, S. X-Ray structure elucidation of a Pt-metalloporphyrin and its application for obtaining sensitive AuNPs-plasmonic hybrids capable to detect triiodide anions. *Int. J. Mol. Sci.* **2019**, *20*, 710. [[CrossRef](#)] [[PubMed](#)]
43. Fringu, I.; Lascu, A.; Macsim, A.M.; Fratilescu, I.; Epuran, C.; Birdeanu, M.; Fagadar-Cosma, E. Pt(II)-A2B2 metalloporphyrin-AuNPs hybrid material suitable for optical detection of 1-anthraquinonesulfonic acid. *Chem. Pap.* **2022**, *76*, 2513–2527. [[CrossRef](#)]
44. Umezawa, Y.; Buhmann, P.; Umezawa, K.; Tohda, K.; Amemiya, S. Potentiometric selectivity coefficients of ion-selective electrodes. Part. I. Inorganic cations. *Pure Appl. Chem.* **2002**, *74*, 923–994. [[CrossRef](#)]
45. Öztürk, N.; Çırak, Ç.; Bahçeli, S. FT-IR Spectroscopic Study of 1,5-Pentanedithiol and 1,6-Hexanedithiol Adsorbed on NaA, CaA and NaY Zeolites. *Z. Naturforsch.* **2014**, *60*, 633–636. [[CrossRef](#)]
46. Wen, P.; Gong, P.; Mi, Y.; Wang, J.; Yang, S. Scalable fabrication of high quality graphene by exfoliation of edge sulfonated graphite for supercapacitor application. *RSC Adv.* **2014**, *4*, 35914–35918. [[CrossRef](#)]
47. Boukir, A.; Fellak, S.; Doumenq, P. Structural characterization of *Argania spinosa* Moroccan wooden artifacts during natural degradation progress using infrared spectroscopy (ATR-FTIR) and X-ray diffraction (XRD). *Heliyon* **2019**, *5*, e02477. [[CrossRef](#)]
48. Wang, M.Y.; Zhu, W.; Wang, Q.; Yang, Y.; Zhou, H.; Zhang, F.; Zhou, L.; Razal, J.M.; Wallace, G.G.; Chen, J. Metal porphyrin intercalated reduced graphene oxide nanocomposite utilized for electrocatalytic oxygen reduction. *Green Energy Environ.* **2017**, *2*, 285–293. [[CrossRef](#)]
49. Chen, B.-K.; Su, C.-T.; Tseng, M.-C.; Tsay, S.-Y. Preparation of Polyetherimide Nanocomposites with Improved Thermal, Mechanical and Dielectric Properties. *Polym. Bull.* **2006**, *57*, 671–681. [[CrossRef](#)]
50. Mak, C.A.; Pericas, M.A.; Fagadar-Cosma, E. Functionalization of A<sub>3</sub>B-type porphyrin with Fe<sub>3</sub>O<sub>4</sub> MNPs. Supramolecular assemblies, gas sensor and catalytic applications. *Catal. Today* **2018**, *306*, 268–275. [[CrossRef](#)]
51. Wei, X.; Du, X.; Chen, D.; Chen, Z. Thermal analysis study of 5,10,15,20-tetrakis (methoxyphenyl) porphyrins and their nickel complexes. *Thermochim. Acta* **2006**, *440*, 181–187. [[CrossRef](#)]
52. Elghamry, I.; Ibrahim, S.S.; Abdelsalam, M.; Al-Faiyz, Y.; Al-Qadri, M. Synthesis, Thermal Stability and Electrocatalytic Activities of meso-tetrakis (5-bromothiophen-2-yl) Porphyrin and Its Cobalt and Copper Complexes. *Int. J. Electrochem. Sci.* **2018**, *13*, 10233–10246. [[CrossRef](#)]
53. Pinto, V.H.A.; CarvalhoDa-Silva, D.; Santos, J.L.M.S.; Weitner, T.; Fonseca, M.G.; Yoshida, M.I.; Idemori, Y.M.; Batinić-Haberle, I.; Rebouças, J.S. Thermal stability of the prototypical Mn porphyrin-based superoxide dismutase mimic and potent oxidative-stress redox modulator Mn(III) meso-tetrakis(N-ethylpyridinium-2-yl)porphyrin chloride, MnTE-2-PyP5+. *J. Pharm. Biomed. Anal.* **2013**, *25*, 29–34. [[CrossRef](#)]
54. Yajima, T.; Maccarrone, G.; Takani, M.; Contino, A.; Arena, G.; Takamido, R.; Hanaki, M.; Funahashi, Y.; Odani, A.; Yamauchi, O. Combined effects of electrostatic and pi-pi stacking interactions: Selective binding of nucleotides and aromatic carboxylates by platinum(II)-aromatic ligand complexes. *Chemistry* **2003**, *9*, 3341–3352. [[CrossRef](#)]
55. Dimitrijević, B.P.; Borozan, S.Z.; Stojanović, S.D.  $\pi$ - $\pi$  and cation- $\pi$  interactions in protein-porphyrin complex crystal structures. *RSC Adv.* **2012**, *2*, 12963. [[CrossRef](#)]
56. Almeida, S.A.A.; Heitor, A.M.; Montenegro, M.C.B.S.M.; Sales, M.G.F. Sulfadiazine-selective determination in aquaculture environment: Selective potentiometric transduction by neutral or charged ionophores. *Talanta* **2011**, *85*, 1508–1516. [[CrossRef](#)] [[PubMed](#)]
57. Santos, E.M.G.; Araújo, A.N.; Couto, C.M.C.M.; Montenegro, M.C.B.S.M. Potentiometric behaviour of ion selective electrodes based on iron porphyrins: The influence of porphyrin substituents on the response properties and analytical determination of diclofenac in pharmaceutical formulations. *J. Pharm. Biomed. Anal.* **2006**, *42*, 535–542. [[CrossRef](#)] [[PubMed](#)]
58. Hasheminejad, M.; Nezamzadeh-Ejhieh, A. A novel citrate selective electrode based on surfactant modified nano-clinoptilolite. *Food Chem.* **2015**, *172*, 794–801. [[CrossRef](#)]
59. Nooredeen, N.M.; Abd El-Ghaffar, M.A.; Darwish, W.M.; Elshereafy, E.; Radwan, A.A.; Abbas, M.N. Graphene oxide with covalently attached zinc monoamino-phthalocyanine coated graphite electrode as a potentiometric platform for citrate sensing in pharmaceutical preparations. *J Solid State Electrochem.* **2015**, *19*, 2141–2154. [[CrossRef](#)]

60. Ribeiro, C.M.F.; Matos, C.D.; Sales, M.G.F.; Vaz, M.C.V.F. Citrate selective electrodes for the flow injection analysis of soft drinks, beers and pharmaceutical products. *Anal. Chim. Acta* **2002**, *471*, 41–49. [[CrossRef](#)]
61. Mazloun-Ardakani, M.; Hoseynidokht, F.; Zare, H.R.; Vafazadeh, R. Development of a Polymeric Membrane Electrode for Determination of Citrate Ions by Potentiometric Technique. *Anal. Bioanal. Electrochem.* **2018**, *10*, 1093–1107.

**Disclaimer/Publisher’s Note:** The statements, opinions and data contained in all publications are solely those of the individual author(s) and contributor(s) and not of MDPI and/or the editor(s). MDPI and/or the editor(s) disclaim responsibility for any injury to people or property resulting from any ideas, methods, instructions or products referred to in the content.